ANNALS of Clinical and Translational Neurology
Open Access
AMERICAN NEUROLOGICAL ASSOCIATION

RESEARCH ARTICLE

Cardiovascular factors are related to dopamine integrity and cognition in aging

Nina Karalija[1,2], Anders Wåhlin[1,2], Jesper Ek[1,2], Anna Rieckmann[1,2], Goran Papenberg[3], Alireza Salami[2,3,4,5], Andreas M. Brandmaier[6,7,8], Ylva Köhncke[6,7,8], Jarkko Johansson[1,2], Micael Andersson[2,4], Jan Axelsson[1,2], Greger Orädd[1,2], Katrine Riklund[1,2], Martin Lövdén[3], Ulman Lindenberger[6,7,8], Lars Bäckman[3] & Lars Nyberg[1,2,4]

[1]Department of Radiation Sciences, Diagnostic Radiology, Umeå University, S-90187, Umeå, Sweden
[2]Umeå Center for Functional Brain Imaging (UFBI), Umeå University, S-90187, Umeå, Sweden
[3]Aging Research Center, Karolinska Institutet & Stockholm University, Tomtebodavägen 18A,S-17165, Stockholm, Sweden
[4]Department of Integrative Medical Biology, Umeå University, S-90187, Umeå, Sweden
[5]Wallenberg Center for Molecular Medicine, Umeå University, Umeå, Sweden
[6]Center for Lifespan Psychology, Max Planck Institute for Human Development, Lentzeallee 94,D-14195, Berlin, Germany
[7]Max Planck, UCL Centre for Computational Psychiatry and Ageing Research, Berlin, Germany
[8]Max Planck, UCL Centre for Computational Psychiatry and Ageing Research, London, United Kingdom

Correspondence
Nina Karalija, Department of Radiation Sciences, Diagnostic Radiology, Umeå University, SE-90187 Umeå, Sweden.
Tel: +46704985147; Fax: +46090133607;
E-mail: nina.karalija@umu.se

Funding Information
This work was funded by the Swedish Research Council, Umeå University, Umeå University–Karolinska Institute Strategic Neuroscience Program, the Knut and Alice Wallenberg Foundation, the Torsten and Ragnar Söderberg Foundation, an Alexander von Humboldt Research award, a donation from the Jochnick Foundation, Swedish Brain Power, the Swedish Brain Foundation, Västerbotten County Council, Innovation Fund of the Max Planck Society, and Gottfried Wilhelm Leibniz Research Award 2010 of the German Research Foundation (DFG).

Received: 2 September 2019; Accepted: 25 September 2019

Annals of Clinical and Translational Neurology **2019; 6(11): 2291–2303**

doi: 10.1002/acn3.50927

Abstract

Objective: The aging brain undergoes several changes, including reduced vascular, structural, and dopamine (DA) system integrity. Such brain changes have been associated with age-related cognitive deficits. However, their relative importance, interrelations, and links to risk factors remain elusive. **Methods**: The present work used magnetic resonance imaging and positron emission tomography with ^{11}C-raclopride to jointly examine vascular parameters (white-matter lesions and perfusion), DA D2-receptor availability, brain structure, and cognitive performance in healthy older adults (n = 181, age: 64–68 years) from the Cognition, Brain, and Aging (COBRA) study. **Results**: Covariance was found among several brain indicators, where top predictors of cognitive performance included caudate and hippocampal integrity (D2DR availability and volumes), and cortical blood flow and regional volumes. White-matter lesion burden was negatively correlated with caudate DA D2-receptor availability and white-matter microstructure. Compared to individuals with smaller lesions, individuals with confluent lesions (exceeding 20 mm in diameter) had reductions in cortical and hippocampal perfusion, striatal and hippocampal D2-receptor availability, white-matter microstructure, and reduced performance on tests of episodic memory, sequence learning, and processing speed. Higher cardiovascular risk as assessed by treatment for hypertension, systolic blood pressure, overweight, and smoking was associated with lower frontal cortical perfusion, lower putaminal D2DR availability, smaller grey-matter volumes, a larger number of white-matter lesions, and lower episodic memory performance. **Interpretation**: Taken together, these findings suggest that reduced cardiovascular health is associated with poorer status for brain variables that are central to age-sensitive cognitive functions, with emphasis on DA integrity.

Introduction

The aging brain undergoes numerous changes, affecting the integrity of the cerebrovascular system, grey- and white matter, and neurochemistry.[1–3] These alterations likely underlie age-related cognitive deficits, and the large inter-individual variability observed therein.[4] Still, their

interrelations and relative importance for cognitive status in old age remain unclear.

Age-related changes in the cerebrovascular system include structural reorganization of the vascular beds, reduced vessel elasticity, and disintegration of the blood-brain barrier.[5,6] Further observations include reduced cerebral perfusion,[7] and increased lesion burden in the cerebral white matter.[8,9] Lesions can be observed as white-matter hyperintensities (WMHs) upon magnetic resonance imaging (MRI).[10] They arise from ischemia, hypoperfusion, blood-brain-barrier breakage, and inflammation and are considered manifestations of cerebral small-vessel disease.[11] WMHs are highly prevalent in aging and predictive of broad-ranged cognitive decline, dementia, and mortality.[12]

Dopamine (DA) has been identified as an important modulator of cognitive functions. Maladaptive DA signaling typically gives rise to cognitive impairment, whereas increased DA transmission, if not excessive, may improve performance.[13,14] Numerous positron emission tomography (PET) studies have demonstrated reduced availability of DA constituents in older individuals,[15] with links to reduced cognitive performance.[1] The age sensitivity of the DA system has therefore been suggested to modulate cognitive trajectories in aging.

Research suggests relationships among vascular function, DA status, and atrophy in pathological and normal aging. Parkinsonian diseases (PD) and schizophrenia have been characterized by DA malfunction and concomitant white-matter abnormalities,[16,17] but also altered perfusion,[18,19] disintegration of the blood-brain barrier,[20,21] and atrophy.[22,23] Cognitive impairments in PD have been related to deficits in perfusion and DA decline,[24] which are exacerbated in presence of WMHs.[25] Increased WMH burden in normal aging is paralleled by decreased grey- and white-matter volume,[8] and has been associated with reduced DA transporter and D1 receptor availability.[26] Although covariance has been observed among several neural measures in non-pathological aging, with links to cognition,[14,26,27] shortage of multimodal studies, and especially studies of DA, leaves their relationships and roles in cognitive aging unclear.

We evaluated the interrelation among WMH burden, cerebral perfusion, DA D2-receptor (D2DR) availability, grey- and white-matter structure, and cognition in 181 healthy, older adults (age: 64–68 years). We hypothesized that WMH burden would be linked to DA system integrity, structural brain measures, and cognition. Second, as predicted by the brain-maintenance account,[4] we expected more prominent effects on cognition in individuals with reductions in several brain measures. Third, due to previous indications of cardiovascular risk factors giving rise to diminished vascular, brain, and cognitive status,[2,3] we hypothesized that cardiovascular disease risk[28] would predict neurocognitive status.

Methods

Sample

This study was carried out in accordance with the Declaration of Helsinki. Informed consent was obtained prior to any testing.

The analyses were conducted using data from the Cognition, Brain, and Aging (COBRA) study in which healthy, older adults (n = 181, age: 64–68 years, 100 men) have undergone ^{11}C-raclopride/PET, MRI, cognitive testing, and lifestyle mapping (Fig. 1). Participants were randomly selected from the population registry of Umeå in Sweden. Exclusion criteria were factors that affect brain and cognitive functions, including cognitive impairment, brain pathology, mental and physical disability, certain medications, and MRI-inhibiting factors. A Mini-Mental State Examination (required: 27 of 30) and radiological evaluation of MR images served as objective measures. We refer to a detailed description of the COBRA study for further details.[29]

Volumetric assessments

MRI was performed with a 3 Tesla Discovery MR 750 scanner (General Electric, WI, US), equipped with a 32-channel phased-array head coil. A 3D fast spoiled gradient-echo sequence was used to obtain high-resolution anatomical T1-weighted images. Imaging parameters were 176 sagittal slices, with slice thickness = 1 mm, TR = 8.2 msec, TE = 3.2 msec, flip angle = 12°, and field of view = 25 × 25 cm.

Subcortical brain structures were delineated with the Freesurfer 5.3. software (http://surfer.nmr.mgh.harvard.edu,[30] and cortical parcellation was performed according to the Desikan-Killiany atlas.[31] Voxel Edit mode in Freeview was used to correct putaminal volumes manually when necessary. The number of voxels within delineated structures represented grey- and white-matter volumes. Frontal cortex volume was the sum of all frontal subregions.[31] Before entered into analyses, the raw volumes were corrected for total intracranial volume (ICV; defined as the sum of volumes for grey and white matter, and cerebrospinal fluid): adjusted volume = raw volume − b(ICV – mean ICV), where b is the slope of regression of volume on ICV.[32]

White-matter microstructure and lesions

Diffusion tensor imaging (DTI) was used to assess white-matter microstructure. Images were acquired by a spin-echo-planar T2-weighted sequence, with 3 repetitions and 32 independent directions. The total slice

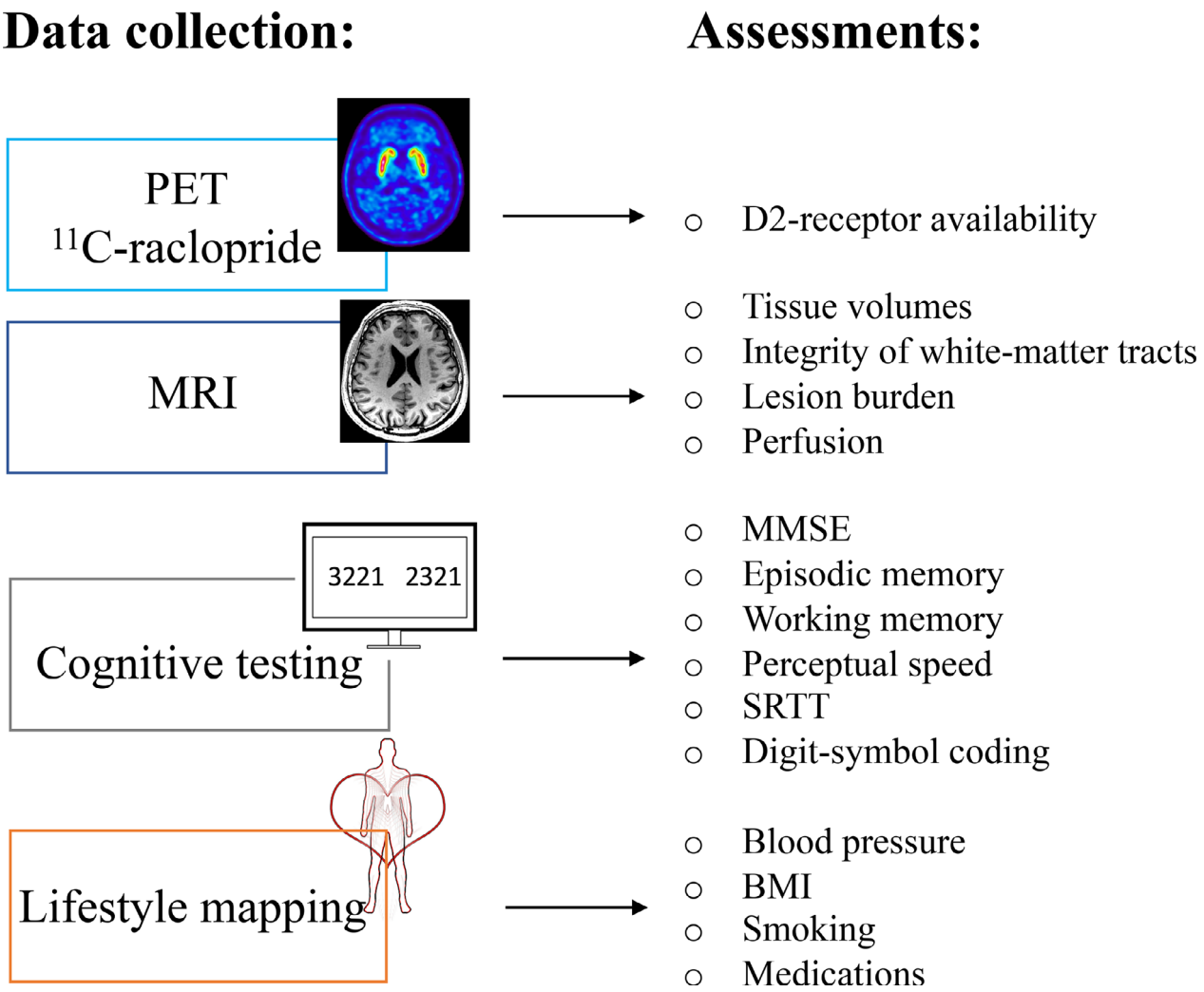

Figure 1. Overview of the data collection and the variables assessed in the present work. PET: positron emission tomography; MRI: magnetic resonance imaging; SRTT: serial-reaction time test; MMSE: Mini Mental State Examination.

number was 64, with TR = 8000 msec, TE = 84.4 msec, flip angle = 90°, field of view = 25 × 25 cm, and b = 1000 sec/mm^2.

DTI data analysis was performed using the FMRIB Software Library (FSL) package (http://www.fmrib.ox.ac.uk/fsl) and Tract-Based Spatial Statistics (TBSS) as part of the FMRIB software package. The three subject-specific diffusion acquisitions were concatenated in time followed by eddy-current correction. Accordingly, the b-matrix was reoriented based on the transformation matrix.[33] The first volume within the averaged volume that did not have a gradient applied (i.e. the first b = 0) was used to generate a binary brain mask with the Brain Extraction Tool.[34] Finally, DTIfit was used to fit a diffusion tensor to each voxel included in the brain mask/space, yielding voxel-wise maps of fractional anisotropy (FA). Using the TBSS processing stream, all subject-specific FA maps were nonlinearly normalized to standard space and then fed into a skeletonize program to make a skeleton of common white-matter tracts across all subjects. Mean diffusivity (MD) images were processed based on the results of the processing of the FA images, yielding individual MD skeletons. Averaged FA and MD along the spatial course of the entire skeleton were computed with reference to JHU ICBM-DTI-81 white matter labels.[35]

A fluid-attenuated inversion recovery (FLAIR) sequence was acquired to assess WMH burden. The total number of slices were 48, slice thickness = 3 mm, TE = 120 msec, TR = 8000 msec, and field of view = 24 × 24 cm.

WMHs were segmented by the lesion growth algorithm[36] as implemented in the LST toolbox version 2.0.14 (www.statisticalmodelling.de/lst.html) for SPM12. First, the algorithm segmented the T1 images into the three main tissue classes (cerebrospinal fluid, grey matter, and

white matter). This information was combined with the coregistered FLAIR intensities to calculate lesion belief maps. By thresholding these maps with a pre-chosen initial threshold ($\kappa = 0.3$, defined by visual inspection), an initial binary lesion map was obtained. This map was then grown along hyperintense neighboring voxels in the FLAIR image, resulting in a lesion probability map, that after thresholding (50%), yielded a binary map of lesions from which the total volume (cm^3) and number of lesions per individual was obtained.

Moreover, the size of the largest WMH was measured for each individual.[9] Accordingly, individuals were assigned into grade 1 if lesion diameters were ≤9 mm (or grouped lesions <20 mm), grade 2 if lesion diameters were 10–20 mm (or grouped lesions >20 mm with connecting bridges between individual lesions), or grade 3 if lesions or confluent areas of hyperintensity were >20 mm.

Perfusion measurements

Perfusion measurements were performed with 3D pseudo-continuous arterial spin labeling (3D pcASL) acquired with background suppression and a spiral readout. Labeling time = 1.5 sec, postlabeling delay time = 1.5 sec, field of view = 24 cm, slice thickness = 4 mm, and acquisition resolution = 8 × 512 (arms × data points), with the number of averages set at 3. This sequence provided whole-brain perfusion in mL/100 g/min. Total scanning time was approximately 5 min.

Quantitative perfusion maps were calculated using a postprocessing tool installed on the scanner by the manufacturer. Mean perfusion for the regions of interest (ROIs) were calculated using the Freesurfer segmentation.

D2DR availability

A 55-min, 18-frame dynamic PET scan was acquired during resting-state conditions with a Discovery PET/CT 690 (General Electric, WI, US). An intravenous bolus injection of 250 MBq ^{11}C-raclopride. A CT scan (20 mA, 120 kV, 0.8 sec/revolution) preceded tracer injection for attenuation-correction purposes. Attenuation- and decay-corrected images (47 slices, field of view = 25 cm, 256 × 256-pixel transaxial images, voxel size = 0.977 × 0.977 × 3.27 mm^3) were reconstructed with the iterative algorithm VUE Point HD-SharpIR (GE Healthcare) using 6 iterations, 24 subsets, 3.0 mm post filtering, yielding full width at half maximum (FWHM) of 3.2 mm. Head movements were minimized with individually fitted thermoplastic masks attached to the bed surface.

PET image data were converted from DICOM to NIfTI format and corrected for head movement. The PET and T1 images were co-registered with the Statistical Parametric Mapping software (SPM8). ^{11}C-raclopride binding potential (BP_{ND}) was calculated from time-activity curves for each voxel with orthogonal regression reference Logan analysis[37] within Freesurfer-segmented ROIs, with cerebellar grey matter as the reference area. To minimize the influence of extreme values, median BP_{ND} per ROI was entered into analyses.

Cognitive assessment

Episodic memory was assessed with tests of word recall, number-word recall, and object-position recall (two trials for each task; max scores: 32, 16, and 24 respectively). Working memory was tested with a letter-updating task, a columnized numerical 3-back task, and a spatial-updating task (16, 4, and 10 trials per task; max scores: 48, 108, and 30 respectively). Perceptual speed was assessed with a letter-, number-, and a figure-comparison task (two trials for each task), from which a score of correct responses per minute was calculated. For each of the nine tests, scores were summarized across the total number of blocks or trials and standardized to form composites (T score: mean = 50; SD = 10). Then, for each construct (episodic memory, working memory, and perceptual speed), the respective three sum scores were averaged to create one composite score. Missing values (<1.2% for all variables) were replaced by the average of the available observed scores.

Sequence learning was examined via the serial-reaction time test (SRTT). The task consisted of pressing, as quickly as possible, a key that spatially corresponded to a square on the screen when that square changed color. The experimental trials consisted of 6 blocks, where blocks 1–4 and 6 consisted of identical sequences, whereas block 5 was built up by new sequences. The difference in reaction times between repeated and new sequences (block 5 – (block 4 + block 6)/2), was used as the measure of sequence learning.

Digit-symbol coding, obtained from the Wechsler Adult Intelligence Scale (WAIS), was performed during 90 sec (1 point per correct item coding).

Cardiovascular risk score

Risk factors were aggregated into a multivariable risk score, in accordance with previous descriptions based on findings from the Framingham Heart Study.[28] Factors included age, sex, treatment for hypertension, systolic blood pressure, body mass index (BMI), and smoking. We computed risk estimates with the algorithm proposed by D'Agostino et al. (2008) based on Cox proportional-hazard regression models predicting the risk (as probability) to develop any form of cardiovascular disease during

a 10-year period (based on cardiovascular disease risk during a 10-year period in 8,491 individuals of ages 30–74 years without cardiovascular disease at baseline):

$$\hat{p} = 1 - S_0(t)\exp\left(\sum_{i=1}^{m}\beta_i\left(X_i - \overline{X_i}\right)\right)$$

with S0(t) being the baseline survival at follow-up time t (t = 10 years), βi the estimated regression coefficient, X_i the log-transformed value of the ith risk factor, $\overline{X}_i$ the corresponding mean, and m the number of risk factors considered. Baseline survival, means, and regressions coefficients were taken from the original algorithm and we inserted the participants' risk variables to compute scores. Risk score calculators are found at framinghamheartstudy.org.

Statistical evaluation

Statistical analyses were conducted using SPSS Statistics software (version 24). Brain and cognitive parameters were normally distributed (skewness: -.55 to .91, kurtosis: -.38 to 1.43), except for WMH burden (skewness: 2.56 and 3.38, kurtosis: 8.27 and 22.2 for lesion volume and number of lesions, respectively; Fig. 2A and B). WMH burden displayed large inter-individual variability (mean: 2.7 ± 1.9 cm^3 and 31.9 ± 20.1 number of lesions; an example of high lesion burden is displayed in Fig. 2C). Only one individual had no lesions at all. An approximately normal distribution for WMH burden was achieved by transforming values with the natural logarithm (resulting skewness: −0.84 and −1.18, kurtosis: 1.18 and 5.52 for

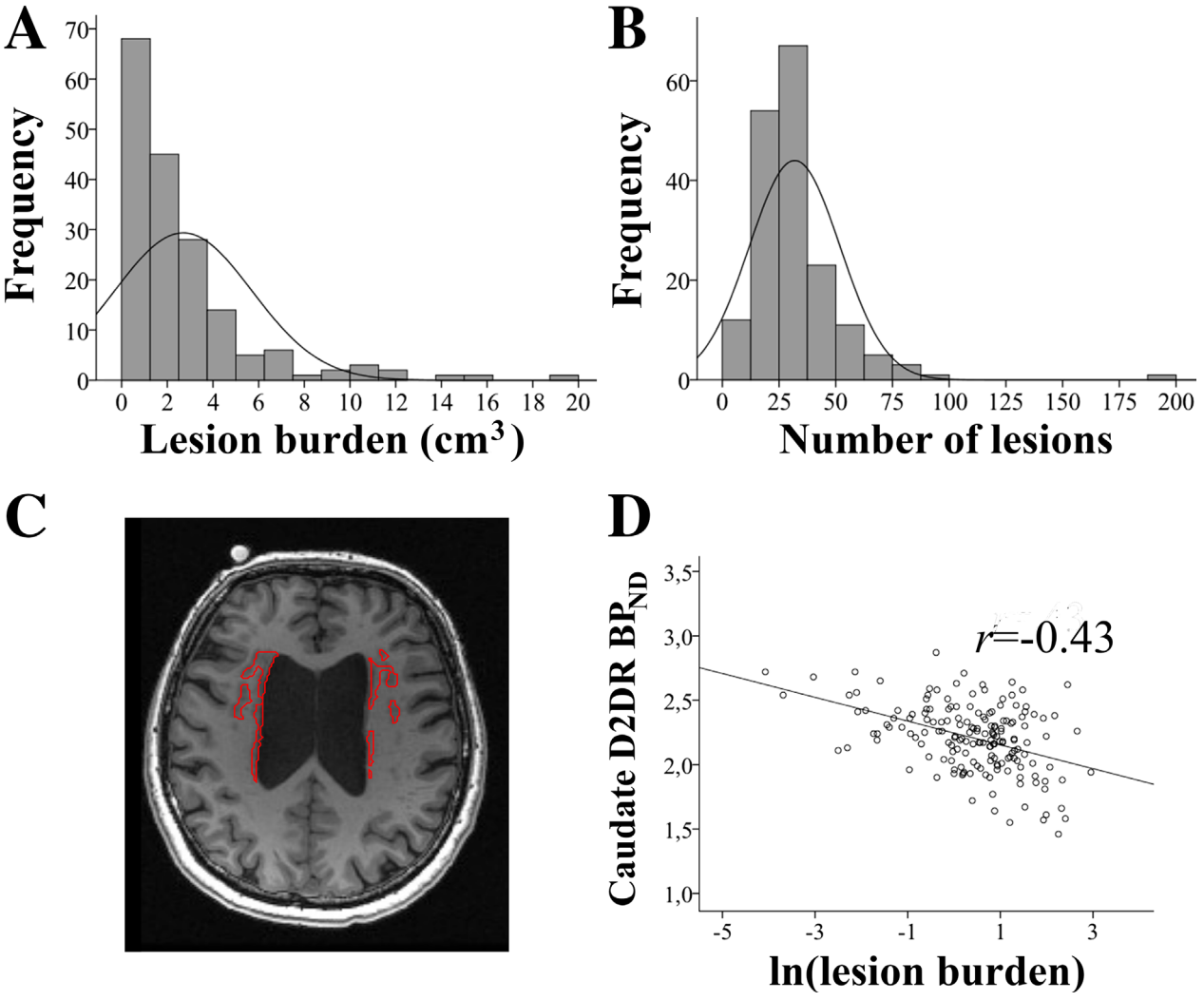

Figure 2. White-matter lesion burden (A: volume in cm^3; B: number of lesions) for the COBRA sample, in which a subset had lesion burden in the high-end range (example in C). Lesion burden was negatively associated with caudate D2DR availability (BP_{ND}; D).

Table 1. Zero-order correlations among white-matter hyperintensity (WMH) burden and measures of perfusion, D2DR availability (BP_{ND}), brain structure, and cognition.

	WMH burden	
	cm^3	Number of lesions
Perfusion		
Putamen	−0.11	−0.11
Caudate	−0.18*	−0.15
Hippocampus	−0.11	−0.10
Frontal cortex	−0.20**	−0.23**
D2DR BP_{ND}		
Putamen	−0.14	−0.14
Caudate	**−0.43*****	**−0.32*****
Hippocampus	−0.17*	−0.14
Volumes		
Putamen	0.07	0.10
Caudate	0.12	0.06
Hippocampus	0.09	0.03
Frontal cortex	0.12	0.10
Cortex (tot)	0.12	0.09
White matter (tot)	0.14	0.10
DTI		
Entire skeleton		
FA	−0.20**	−0.18*
MD	**0.34*****	**0.31*****
Cognition		
Episodic memory	−0.13	−0.14
Working memory	−0.02	0.05
Perceptual speed	−0.01	−0.11
SRTT	0.17*	0.12
Digit-symbol coding	−0.09	−0.11

Correlations surviving Holm-Bonferroni corrections are presented in bold font. DTI, diffusion tensor imaging; FA, fractional anisotropy; MD, medial diffusivity; SRTT, serial-reaction time test.
*$P < 0.05$.
**$P < 0.01$.
***$P < 0.001$.

lesion volume and number of lesions, respectively), which were used throughout analyses (e.g. Fig. 2D).

Descriptive data are presented as frequencies, or mean values and standard deviations (SD). Correlations are reported as the Pearson correlation coefficient (r). In order to control the false-positive rate, we corrected for multiple comparisons using the Holm-Bonferroni method, where $k = 20$ for Table 1, and $k = 22$ for Table 4.

To test the predictive power of individual lesion size, neurocognitive differences were tested among groups with white-matter lesion graded as 1–3 with multivariate analysis of variance (MANOVA) followed by Bonferroni-corrected follow-up tests (Table 2).

The independent and joint contributions of the brain indicators in Table 1 for cognitive functioning were assessed with partial least-squares (PLS) regression. PLS regression combines the features of principal component analysis and multiple regression and is preferable when multicollinearity exists among predictors and there is a risk of over-fitting the model. The number of observed variables (here 17 brain variables) are reduced into a few latent factors that are tested for linear relationships with cognitive performance (via R^2 and adjusted R^2). For each brain variable, their loading onto the latent factors and their regression weights are reported for predicting cognitive performance in Table 3, hence demonstrating the (adjusted) variance explained by the factor and the individual importance per variable.

Furthermore, to investigate whether the previously reported DA-cognition relationships[38] are modulated by white-matter lesion burden (e.g. further assessing the second hypothesis stipulated in the introduction), interactions were tested between WMH burden and caudate and hippocampal D2DR availability for cognitive performance using multiple linear regression.

The contribution of cardiovascular risk factors for neurocognitive status was estimated with multivariate linear regression with cardiovascular risk as the independent variable, and WMHs, perfusion, BP_{ND}, volume, white-matter microstructure, and cognition as dependent variables.

Exclusions were handled using pairwise deletions and concerned values for striatal BP_{ND} ($n = 7$), striatal volumes ($n = 2$), and hippocampal BP_{ND} and volumes ($n = 3$), and cardiovascular risk scores> 66 ($n = 1$), due to imperfect segmentation of MR images, problems with PET/MR co-registration, observations of extensive grey matter atrophy, or for being statistical outliers according to the outlier labeling rule with 2.2 interquartile ranges. There were a few missing cases for measures of WMHs ($n = 4$) and DTI ($n = 3$).

Results

Neurocognitive correlates of white-matter lesions

We hypothesized that WMH burden would be linked to DA system integrity, structural brain measures, and cognition. To test this, we first examined zero-order correlations among WMH burden (expressed as volume and as number of lesions, interrelation: $r = 0.75$, $P < 0.001$) and perfusion, D2DR availability, grey- and white-matter structure, and cognitive performance (Table 1). Following control for multiple comparisons, significant associations were found between WMH burden and caudate D2DR availability ($r = -0.43$ for lesion volume, Fig. 2D; and $r = -0.32$ for number of lesions), and between WMH burden and MD for the white-matter skeleton ($r = 0.34$ for lesion volume, and $r = 0.31$ for number of lesions). No significant associations were found between WMH burden and grey-matter volumes. Notably, caudate D2DR availability was not correlated with caudate perfusion ($r = 0.08$, $P > 0.05$), and the link

Table 2. Comparisons of neurocognitive status in individuals with varying size of white-matter lesions.

White-matter lesion size			
	Grade 1	Grade 2	Grade 3
Perfusion			
Putamen	45.97 ± 6.43	46.20 ± 7.60	43.73 ± 5.85
Caudate	44.65 ± 6.23	**44.49 ± 7.23***	40.80 ± 4.65
Hippocampus	40.93 ± 7.29	**41.89 ± 7.66***	37.22 ± 5.79
Frontal cortex	**45.20 ± 7.75***	**44.29 ± 10.33***	38.21 ± 6.29
D2DR BP_{ND}			
Putamen	**3.39 ± 0.27****	**3.34 ± 0.25***	3.17 ± 0.32
Caudate	**2.32 ± 0.25*****	**2.22 ± 0.22*****	1.95 ± 0.32
Hippocampus	0.26 ± 0.04	**0.27 ± 0.05***	0.24 ± 0.05
Volumes (cm^3)			
Putamen	4.31 ± 0.47	4.43 ± 0.50	4.52 ± 0.64
Caudate	3.64 ± 0.42	3.63 ± 0.46	3.81 ± 0.72
Hippocampus	3.90 ± 0.48	3.87 ± 0.37	3.86 ± 0.52
Frontal cortex	163.55 ± 18.70	164.99 ± 14.83	162.52 ± 19.99
Cortex (tot)	446.43 ± 50.34	452.27 ± 38.30	437.87 ± 61.64
White matter	602.38 ± 64.93	604.44 ± 58.39	604.06 ± 62.98
DTI			
Entire skeleton			
FA	**0.479 ± 0.013****	**0.475 ± 0.015****	0.464 ± 0.018
MD	**0.769 × 10^{-3} ± 0.016*****	**0.777 × 10^{-3} ± 0.022****	0.795 ± 0.026 × 10^{-3}
Cognition			
Episodic memory	**51.59 ± 7.59***	50.06 ± 8.22	46.19 ± 5.53
Working memory	49.98 ± 7.09	50.51 ± 7.74	47.21 ± 6.75
Perceptual speed	50.14 ± 9.12	49.88 ± 8.29	50.25 ± 9.43
SRTT	**22.07 ± 33.06**$^{\#\#}$	39.62 ± 31.62	33.29 ± 26.55
Digit-symbol coding	37.78 ± 8.82	**38.26 ± 7.78***	33.46 ± 7.83

grade 1: <10 mm, $n = 41$; grade 2: 10–20 mm, $n = 112$; or grade 3: >20 mm, $n = 24$. Significant between-group differences are presented in bold font. *$P < 0.05$, **$P < 0.01$, ***$P < 0.001$ for grade 1 or 2 compared to grade 3; $^{\#\#}P < 0.01$ grade 1 compared to grade 2. SSRT: serial-reaction time test.

between WMH burden and caudate D2DR availability remained when controlling for caudate perfusion, age, and caudate volume ($rs = -0.42$ to -0.43, $P < 0.001$ for all).

Next, we evaluated neurocognitive differences among groups with small- compared to larger-sized lesions (grade 1–3; Table 2). Individuals with the largest lesions had the highest total WMH burden, both in terms of total lesion volumes (grade 1: 0.56 ± 0.43, grade 2: 2.37 ± 1.46; grade 3: 7.90 ± 4.66 cm^3; $F(2,174) = 99.34$, $P < 0.001$ for all comparisons) and number of lesions (20.7 ± 11.6, 33.3 ± 20.42; 45.4 ± 19.1 for groups; $F(2,174) = 13.73$, $P \leq 0.01$ for all comparisons). Individuals with large, confluent lesions exceeding 20 mm in diameter (grade 3) had lower cerebral perfusion ($F(2, 172) = 3.2$, 4.0, and 4.9 for caudate, hippocampus, and frontal cortex), striatal and hippocampal D2DR availability ($F(2, 166) = 5.06$, 15.6, and 3.6 for putamen, caudate, and hippocampus), white-matter microstructure ($F(2, 171) = 7.3$ and 10.7 for FA and MD across the entire skeleton) compared to individuals with smaller lesions. Furthermore, this group had the lowest performance on tasks of episodic memory ($F(2,173) = 3.7$), sequence learning ($F(2,173) = 4.7$), and digit-symbol coding ($F(2,173) = 3.6$) compared to those with smaller lesions.

Brain predictors of cognitive performance

The contributions of the brain-related variables in Table 1 for cognitive performance were assessed with PLS (Table 3). In the model with episodic memory, the first factor explained 20.9% of the variance among indicators and 7.3% (6.7% based on adjusted R^2) of variance in performance. The top predictors were caudate and hippocampal BP_{ND} and volumes, and frontal cortical perfusion. The second and third factors explained additional 3.6% and 1.6% of variance in performance respectively. For working memory, the first latent factor explained 23.5% of the variance among indicators and 7.5% (6.9% based on adjusted R^2) of variance in performance. The top predictors consisted of white- and grey-matter (cortical and subcortical) volumes. The second and third factors explained additional 1.9% and 1.2% of variance in performance, respectively. In addition, the first factor for the model of perceptual speed explained 18.9% of the variance among brain variables and

Table 3. Brain predictors of cognitive performance. The first factor from partial least-squares regression analyses explained most variance in performance. Individual loadings onto the first factor and importance (via regression weights) are presented for each brain variable.

	Episodic memory		Working memory		Perceptual speed		SRTT		Digit-symbol coding	
	Loadings	Weights	Loadings	Weights	Loadings	Weights	Loadings	Weights	Loadings	Weights
WMH burden										
Volume	−0.24	−0.16	0.07	−0.02	0.14	0.17	0.34	**0.45**	−0.02	−0.08
Number of lesions	−0.23	−0.20	0.07	0.15	0.01	−0.17	0.32	**0.41**	−0.05	−0.16
Perfusion										
Putamen	0.37	0.23	0.27	0.23	0.45	0.**22**	0.11	0.11	0.30	0.25
Caudate	0.39	0.22	0.27	0.24	0.41	−0.06	0.03	0.03	0.30	0.12
Hippocampus	0.37	0.23	0.24	0.13	0.42	0.14	0.29	0.**29**	0.28	0.20
Frontal cortex	0.41	0.**31**	0.22	0.14	0.46	0.**47**	0.15	0.15	0.29	0.27
D2DR BP_{ND}										
Putamen	0.26	0.27	−0.10	−0.21	−0.28	−0.13	−0.09	−0.01	−0.06	−0.10
Caudate	0.35	**0.42**	−0.08	−0.15	−0.30	−**0.39**	−0.15	−0.10	−0.04	0.27
Hippocampus	0.31	**0.38**	0.12	0.22	−0.15	−0.10	0.10	0.26	0.11	0.15
Volumes										
Putamen	0.09	0.06	0.31	**0.34**	0.15	−0.08	0.21	−0.03	0.24	0.16
Caudate	0.13	**0.31**	0.22	0.22	0.34	0.**43**	0.10	−0.16	0.21	**0.27**
Hippocampus	0.28	0.**28**	0.33	**0.32**	0.41	0.**39**	0.33	0.07	0.37	**0.49**
Frontal cortex	0.25	0.21	0.44	**0.36**	0.38	0.08	0.50	**0.35**	0.42	**0.33**
Cortex	0.26	0.18	0.44	**0.35**	0.40	0.11	0.50	**0.46**	0.43	**0.33**
White matter	0.12	−0.20	0.41	**0.41**	0.31	−0.02	0.42	0.25	0.38	**0.35**
DTI										
Entire skeleton										
FA	0.15	−0.02	0.10	0.08	0.13	0.16	0.08	0.05	0.17	0.14
MD	−0.16	−0.01	−0.02	0.06	−0.10	0.05	0.05	0.07	−0.11	−0.03

Numbers are presented in bold font for the five top predictors of respective function. SRTT, serial-reaction time test; DTI, diffusion tensor imaging; FA, fractional anisotropy; MD, medial diffusivity.

only 3.4% (2.8% based on adjusted R^2) of variance in performance. The top predictors were frontal cortical and putaminal perfusion, caudate and hippocampal volume, and caudate BP_{ND}. The second and third factors explained additional 3.7% and 1.3% of variance in performance, respectively. The top predictors of the second factor were caudate volume, BP_{ND}, and perfusion, but also hippocampal volume and frontal cortical perfusion. In the model of SRTT, the first factors explained 4.1% (3.5% based on adjusted R^2) of the variance in performance, and 18.9% of variance among predictors. The top predictors consisted of total cortical and frontal cortical volume, WMH burden (volume and number of lesions), and hippocampal perfusion. The second and third factors explained additional 2.2% and 0.7% of variance in performance, respectively. In the model for digit-symbol coding, the first factor explained 24.1% of the variance among indicators and 6.6% (6.0% based on adjusted R^2) for performance. The top predictors were cortical and subcortical grey-matter and white-matter volumes. The second and third factors explained additional 4.1% and 1.2% of variance in performance, respectively.

In light of the previously reported D2DR-episodic memory association,[38] we performed multiple linear regression analyses to investigate whether WMH burden modulated the association between D2DR availability (in caudate and hippocampus) and cognition. As previously reported (Nyberg et al., 2016), caudate BP_{ND} was a significant predictor of episodic memory performance (here: $\beta = 0.18$, $P = 0.06$). For each cognitive ability, we tested a model with WMH volume, caudate $BP_{ND,}$ and WMH volume × caudate $BP_{ND,}$ as predictors. Each model explained a non-significant portion of the variance in cognitive performance (episodic memory: $F(3,167) = 2.04$, $P = 0.11$, $R^2 = 0.04$; working memory: $F(3,167) = 1.38$, $P = 0.25$; $R^2 = 0.02$; perceptual speed: $F(3,167) = 0.51$, $P = 0.68$, $R^2 = 0.01$; SRTT: $F(3,166) = 1.14$, $P = 0.34$, $R^2 = 0.02$; digit-symbol coding: $F(3,167) = 1.98$, $P = 0.12$; $R^2 = 0.03$). Notably, no significant interaction effects were found ($P > 0.05$ for all WMH volume × caudate BP_{ND}).

The same set of models were performed with hippocampal D2DR availability. A model with hippocampus $BP_{ND,}$, WMH volume, and WMH volume × hippocampus BP_{ND} was predictive of episodic memory ($F(3,172) = 2.91$, $P = 0.04$, $R^2 = 0.05$ (adjusted $R^2 = 0.03$), with a significant effect of hippocampal $BP_{ND,}$ ($\beta = 0.19$, $P = 0.03$), but no effect of volume of white-matter lesions or interactions between lesion volume and D2DR

Table 4. Zero-order correlations among cardiovascular risk and white-matter lesion burden, blood perfusion, D2DR availability (BP_{ND}), brain structure, and cognition.

	Cardiovascular risk
White-matter lesion burden	
Lesion volume	0.05
Number of lesions	0.17*
Perfusion	
Putamen	−0.16*
Caudate	−0.12
Hippocampus	−0.16*
Frontal cortex	**−0.32*** **
D2DR BP_{ND}	
Putamen	−0.16*
Caudate	−0.13
Hippocampus	0.10
Volumes	
Putamen	0.11
Caudate	−0.13
Hippocampus	−0.11
Frontal cortex	0.12
Cortex (tot)	0.10
White matter (tot)	0.20**
DTI	
Entire skeleton	
FA	0.05
MD	0.11
Cognition	
Episodic memory	−0.19*
Working memory	0.09
Perceptual speed	−0.02
SRTT	0.13
Digit-symbol coding	−0.16*

Correlations surviving Holm-Bonferroni corrections are presented in bold font. DTI, diffusion tensor imaging; FA, fractional anisotropy; MD, medial diffusivity; SRTT: serial-reaction time test.
*$P < 0.05$.
**$P < 0.01$.
***$P < 0.001$.

availability. Models for the other cognitive functions were non-significant (working memory: $F(3,172) = 0.82$, $P = 0.48$; $R^2 = 0.01$; perceptual speed: $F(3,172) = 0.26$, $P = 0.85$, $R^2 = 0.01$; SRTT: $F(3,171) = 2.20$, $P = 0.09$, $R^2 = 0.04$; digit-symbol coding: $F(3,172) = 0.70$, $P = 0.56$, $R^2 = 0.01$), and with no predictive value from interactions between lesion volume and D2DR availability ($P > 0.05$). No differences in results were seen when entering number of white-matter lesions instead of WMH volume.

Cardiovascular disease risk is associated with brain status and episodic memory performance

We assessed cardiovascular risk profiles for associations with the whole set of brain and cognitive variables. The cardiovascular risk score (probability multiplied by 100) ranged between 3.5–66.6% (mean: 24.3, SD: 11.2) for the sample and was normally distributed (skewness: 0.77, kurtosis: 0.82; Fig. 3A). Zero-order correlations were found among the risk score and several neurocognitive variables; however, after control for multiple comparisons, only the association between the cardiovascular risk score and frontal cortical perfusion remained (Table 4; Fig. 3B). A multivariate linear regression was performed with cardiovascular risk as the independent variable and the neurocognitive variables in Table 4 as dependent variables. The risk score was predictive of several neurocognitive variables, including reduced frontal cortical perfusion ($F(1,161) = 12.74$, $P < 0.001$; $R^2 = 0.07$, adjusted $R^2 = 0.07$), cortical volume ($F(1161) = 6.82$, $P = 0.01$; $R^2 = 0.04$, adjusted $R^2 = 0.04$), putamen BP_{ND} ($F(1161) = 4.29$, $P = 0.04$; $R^2 = 0.03$, adjusted $R^2 = 0.02$), caudate volume ($F(1161) = 3.79$, $P = 0.05$; $R^2 = 0.02$, adjusted $R^2 = 0.02$), and episodic memory ($F(1161) = 4.95$, $P = 0.03$; $R^2 = 0.03$, adjusted $R^2 = 0.02$). Furthermore, the risk score was associated with increased white-matter volume ($F(1161) = 6.14$, $P = 0.01$; $R^2 = 0.04$, adjusted $R^2 = 0.03$) and at trend level, increased number of white-matter lesions ($F(1161) = 3.58$, $P = 0.06$; $R^2 = 0.02$, adjusted $R^2 = 0.02$).

Discussion

This work examined interrelations among white-matter lesions, white-matter microstructure, D2DR availability, brain volumes, perfusion, cognition, and cardiovascular risk in healthy older adults at an age when cognitive decline typically begins.[4] Shared variance was found among several brain indicators, which were predictive of cognitive performance. Of these, caudate and hippocampal integrity (D2DR availability and volumes), but also cortical perfusion and volumes, constituted principal predictors of cognition. Notably, we found an association between WMH burden and D2DR availability. Individuals with large, confluent WMHs showed broad-ranged reductions in neurocognitive status, including reduced D2DR availability, perfusion, white-matter microstructure, and performance in tasks of episodic memory, sequence learning, and digit-symbol coding. Cardiovascular risk profiles were predictive of several neurocognitive measures, including frontal cortical perfusion, putaminal D2DR availability, grey-matter volumes, number of white-matter lesions, and episodic memory performance.

Research has demonstrated reduction of cerebrovascular integrity, DA markers, and brain volumes in aging and their associations with increased risk of cognitive decline and dementia.[1,2,12] Nevertheless, the interrelation among these brain indicators and their relative links to cognition remain elusive due to shortage of multimodal studies. Episodic memory is particularly age-sensitive and

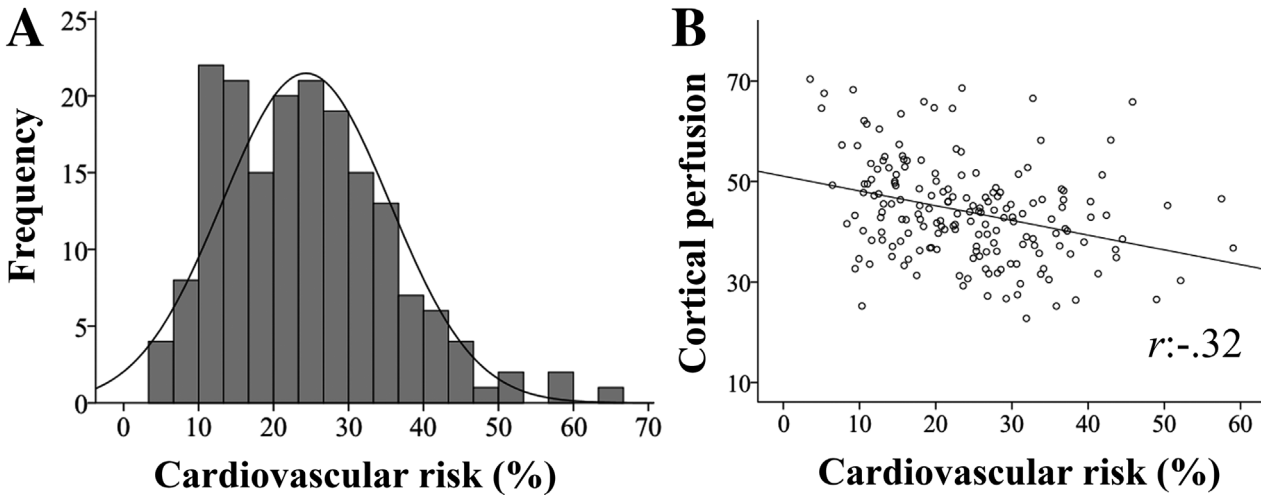

Figure 3. Estimated cardiovascular disease risk within a 10-year period (%, A) and its association with perfusion in the frontal cortex (B). *r*: Pearson's correlation coefficient

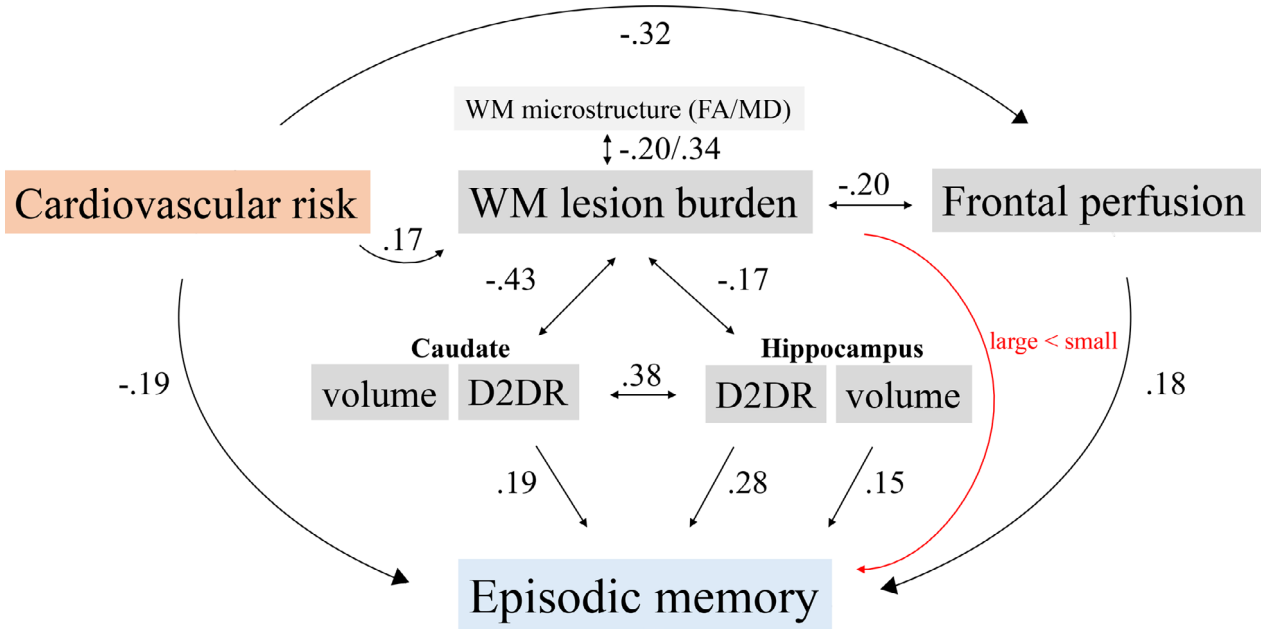

Figure 4. Illustration of the main findings. Associations were found among cardiovascular risk, vascular measures, D2DR availability, and episodic memory. Zero-order correlations are indicated with black single-headed arrows (links to cognition/cardiovascular risk), black doubled-headed arrows (links among brain measures, direction unknown), and a red arrow (lesion size, grade 1–3). FA, fractional anisotropy; MD, medial diffusivity; Cau, caudate; HC, hippocampus.

predicted by D2DR availability.[4,38] We provide evidence for that increased cardiovascular risk is associated with reduced D2DR integrity, frontal cortical blood flow, episodic memory, and increased WMH burden. Furthermore, we show that increased WMH burden correlated negatively with D2DR availability in associative regions, striatum and hippocampus. Although the directionality of the interrelations awaits longitudinal assessments, it seems plausible that cardiovascular risk and vascular dysfunction may modulate the DA-cognition link in aging,[1] as illustrated by an overview of our present and previous[38] results in Figure 4.

The WMH-D2DR link demonstrated here extends findings of reduced DA transporter and D1 receptor

availability in relation to elevated WMH burden.[26] The caudate may be particularly sensitive to ischemic damage, due to its location in regions less likely to receive sufficient blood flow in states of hypoperfusion.[39] Such damage may harm striatal neurons, but also, nigral efferent nerve fibers, thereby reducing D2DR availability, as well as give rise to WMHs. Even though we cannot infer the temporal order of events due to the cross-sectional nature of this study, previous work suggests that reduced cerebrovascular integrity reduces DA-system integrity. For instance, in a longitudinal animal study, induction of cerebral ischemia in rats led to reduced striatal ^{11}C-raclopride binding over time.[40] Another study showed that heart failure was followed by attenuated cerebral blood flow as well as DA levels.[41]

Large heterogeneity in WMH burden was observed, with lower levels in most individuals and higher burden in a subsample. This may reflect the relatively young and narrow age range of our sample, and the rigorous exclusion criteria to include healthy individuals at enrollment.[29] Although computerized WMH segmentation may be successfully achieved,[36] our findings suggest that individual lesion size is more predictive than total burden in identifying individuals with poor neurocognitive status. Indeed, lowest cognitive performance and deterioration in multiple brain parameters were found in individuals with large lesions. This extends previous associations of exacerbated effects of WMHs and DA decline on cognition[25] and is consistent with observations of covariance among several neural measures in normal and pathological aging.[14,16,26,27] As confluent WMHs and reductions in multiple brain indicators are associated with advanced microvascular disease and dementia,[9] the group with the largest lesions may be at risk of an unfortunate aging route.

Increased WMH burden predicts decline in multiple cognitive domains,[42] and has, as in the present work, been linked to reduced episodic memory, sequence learning, and processing speed.[42–44] WMH manifestation constitutes an extreme end of white-matter injury, associated with demyelination, axonal damage, and gliosis,[11] of which earlier signs can be found in DTI-derived measures.[9,45] In line with previous work, WMH burden was predictive of microstructure along the white-matter skeleton,[43] however, not with grey-matter volumes. Furthermore, the DTI-derived measures loaded weakly to the common factor and were not predictive of cognitive performance. These findings may, again, relate to the employment of a healthy sample with relatively low lesion burden. Previously, links between white-matter integrity and cognition have been found in individuals with extensive lesions.[43,46] As performance levels, and change over time, has been found to correlate between various cognitive functions, multivariate PLS may be a viable alternative to describe this multivariate space in future work.

WMHs development are dynamic processes,[47] thus appropriate interventions could modulate their progression. Motivated by previous indication of shared risk factors for brain and cognitive status,[2,3] we assessed individual differences via cardiovascular risk profiles.[28] For instance, systolic blood pressure and BMI have been associated with WMH burden and DA integrity.[8,48,49] Cardiovascular risk estimates were associated with several neurocognitive measures, including perfusion, number of white-matter lesions, D2DR availability, brain volumes, and episodic memory. These results extend previous links between cardiovascular risk profiles and WMHs and cognitive decline in normal aging[8,50] and highlights these factors in the context of successful aging.

Concluding Remarks

As exacerbated brain aging increases the risk for cognitive decline, dementia, and mortality, it is imperative to identify factors associated with successful aging for future intervention strategies. The present cross-sectional data extend our understanding of the interrelation between neurocognitive measures in aging, and that deterioration in such measures partly relies on shared lifestyle-related risk factors. Avoiding the occurrence of large white-matter lesions seems critical, with regard to the broad-ranged neurocognitive reductions demonstrated here. For statements of temporal dynamics and causality, longitudinal measurements from multimodal settings are warranted.

Acknowledgments

This work was funded by the Swedish Research Council, Umeå University, Umeå University–Karolinska Institute Strategic Neuroscience Program, the Knut and Alice Wallenberg Foundation, the Torsten and Ragnar Söderberg Foundation, an Alexander von Humboldt Research award, a donation from the Jochnick Foundation, Swedish Brain Power, the Swedish Brain Foundation, Västerbotten County Council, Innovation Fund of the Max Planck Society, and Gottfried Wilhelm Leibniz Research Award 2010 of the German Research Foundation (DFG).

The Freesurfer analyses were performed on resources provided by the Swedish National Infrastructure for Computing (SNIC) at HPC2N in Umeå.

Author Contributions

K.R., M.L., U.L., and L.B. and L.N. designed and funded the research; N.K. and A.W. performed research and

wrote the manuscript, which was edited by all co-authors. J.E.; A.R.; G.P.; A.S.; A.M.B; Y.K.; and J.J.; analyzed data and/or contributed conceptually. M.A.; J.A.; G.O. analyzed data.

Conflict of Interest

Nothing to report.

References

1. Bäckman L, Nyberg L, Lindenberger U, et al. The correlative triad among aging, dopamine, and cognition: current status and future prospects. Neurosci Biobehav Rev 2006;30:791–807.
2. Raz N, Rodrigue KM. Differential aging of the brain: patterns, cognitive correlates and modifiers. Neurosci Biobehav Rev 2006;30:730–748.
3. Jagust W. Vulnerable neural systems and the borderland of brain aging and neurodegeneration. Neuron 2013;77:219–234.
4. Nyberg L, Lövden M, Riklund K, et al. Memory aging and brain maintenance. Trends Cogn Sci 2012;16:292–305.
5. Lakatta EG, Wang M, Najjar SS. Arterial aging and subclinical arterial disease are fundamentally inter twined at macroscopic and molecular levels. Med Clin North Am 2009;93:583–604.
6. Montagne A, Barnes Samuel R, Sweeney Melanie D, et al. Blood-brain barrier breakdown in the aging human hippocampus. Neuron 2015;85:296–302.
7. Chen JJ, Rosas HD, Salat DH. Age-associated reductions in cerebral blood flow are independent from regional atrophy. NeuroImage 2011;55:468–478.
8. Habes M, Erus G, Toledo JB, et al. White matter hyperintensities and imaging patterns of brain ageing in the general population. Brain 2016;139:1164–1179.
9. Prins ND, Scheltens P. White matter hyperintensities, cognitive impairment and dementia: an update. Nat Rev Neurol 2015;11:157–165.
10. Wardlaw JM, Smith EE, Biessels GJ, et al. Neuroimaging standards for research into small vessel disease and its contribution to ageing and neurodegeneration. Lancet Neurol 2013;12:822–838.
11. Gouw AA, Seewann A, van der Flier WM, et al. Heterogeneity of small vessel disease: a systematic review of MRI and histopathology correlations. J Neurol Neurosurg Psychiatry 2011;82:126–135.
12. Debette S, Markus HS. The clinical importance of white matter hyperintensities on brain magnetic resonance imaging: systematic review and meta-analysis. BMJ 2010;341:c3666.
13. Cools R, D'Esposito M. Inverted-U-shaped dopamine actions on human working memory and cognitive control. Biol Psychiatry 2011;69:e113–e125.
14. Lövden M, Karalija N, Andersson M, et al. Latent-profile analysis reveals behavioral and brain correlates of dopamine-cognition associations. Cereb Cortex 2018;28:3894–3907.
15. Karrer TM, Josef AK, Mata R, et al. Reduced dopamine receptors and transporters but not synthesis capacity in normal aging adults: a meta-analysis. Neurobiol Aging 2017;57:36–46.
16. Bohnen NI, Albin RL. White matter lesions in Parkinson disease. Nat Rev Neurol 2011;7:229–236.
17. Kubicki M, McCarley RW, Shenton ME. Evidence for white matter abnormalities in schizophrenia. Curr Opin Psychiatry 2005;18:121–134.
18. Melzer TR, Watts R, MacAskill MR, et al. Arterial spin labelling reveals an abnormal cerebral perfusion pattern in Parkinson's disease. Brain 2011;134(Pt 3):845–855.
19. Pinkham A, Loughead J, Ruparel K, et al. Resting quantitative cerebral blood flow in schizophrenia measured by pulsed arterial spin labeling perfusion MRI. Psychiatry Res 2011;194:64–72.
20. Pan Y, Nicolazzo JA. Impact of aging, Alzheimer's disease and Parkinson's disease on the blood-brain barrier transport of therapeutics. Adv Drug Deliv Rev 2018;135;62–74.
21. Pollak TA, Drndarski S, Stone JM, et al. The blood-brain barrier in psychosis. Lancet Psychiatry. 2018;5:79–92.
22. van Kammen DP, van Kammen WB, Mann LS, et al. Dopamine metabolism in the cerebrospinal fluid of drug-free schizophrenic patients with and without cortical atrophy. Arch Gen Psychiatry. 1986;43:978–983.
23. Mak E, O'Brien JT, Su L, et al. Baseline and longitudinal grey matter changes in newly diagnosed Parkinson's disease: ICICLE-PD study. Brain 2015;138:2974–2986.
24. Arnaldi D, Campus C, Ferrara M, et al. What predicts cognitive decline in de novo Parkinson's disease? Neurobiol Aging 2012;33:e11–e20.
25. Santangelo G, Vitale C, Trojano L, et al. Differential neuropsychological profiles in Parkinsonian patients with or without vascular lesions. Mov Disord 2010;25:50–56.
26. Rieckmann A, Hedden T, Younger AP, et al. Dopamine transporter availability in clinically normal aging is associated with individual differences in white matter integrity. Hum Brain Mapp 2016;37:621–631.
27. Gorbach T, Pudas S, Lundquist A, et al. Longitudinal association between hippocampus atrophy and episodic-memory decline. Neurobiol Aging 2017;51:167–176.
28. D'Agostino RB Sr, Vasan RS, Pencina MJ, et al. General cardiovascular risk profile for use in primary care: the Framingham Heart Study. Circulation 2008;117:743–753.
29. Nevalainen N, Riklund K, Andersson M, et al. COBRA: a prospective multimodal imaging study of dopamine, brain structure and function, and cognition. Brain Res 2015;1612:83–103.

30. Fischl B, Salat DH, Busa E, et al. Whole brain segmentation: automated labeling of neuroanatomical structures in the human brain. Neuron 2002;33:341–355.
31. Desikan RS, Segonne F, Fischl B, et al. An automated labeling system for subdividing the human cerebral cortex on MRI scans into gyral based regions of interest. NeuroImage 2006;31:968–980.
32. Buckner RL, Head D, Parker J, et al. A unified approach for morphometric and functional data analysis in young, old, and demented adults using automated atlas-based head size normalization: reliability and validation against manual measurement of total intracranial volume. NeuroImage 2004;23:724–738.
33. Leemans A, Jones DK. The B-matrix must be rotated when correcting for subject motion in DTI data. Magn Reson Med 2009;61:1336–1349.
34. Smith SM. Fast robust automated brain extraction. Hum Brain Mapp 2002;17:143–155.
35. Wakana S, Jiang H, Nagae-Poetscher LM, et al. Fiber tract-based atlas of human white matter anatomy. Radiology 2004;230:77–87.
36. Schmidt P, Gaser C, Arsic M, et al. An automated tool for detection of FLAIR-hyperintense white-matter lesions in Multiple Sclerosis. NeuroImage 2012;59:3774–3783.
37. Logan J, Fowler JS, Volkow ND, et al. Distribution volume ratios without blood sampling from graphical analysis of PET data. J Cereb Blood Flow Metab 1996;16:834–840.
38. Nyberg L, Karalija N, Salami A, et al. Dopamine D2 receptor availability is linked to hippocampal-caudate functional connectivity and episodic memory. Proc Natl Acad Sci USA 2016;113:7918–7923.
39. Wodarz R. Watershed infarctions and computed tomography. A topographical study in cases with stenosis or occlusion of the carotid artery. Neuroradiology 1980;19:245–248.
40. Momosaki S, Ito M, Yamato H, et al. Longitudinal imaging of the availability of dopamine transporter and D2 receptor in rat striatum following mild ischemia. J Cereb Blood Flow Metab 2017;37:605–613.
41. Mamalyga ML, Mamalyga LM. Effect of progressive heart failure on cerebral hemodynamics and monoamine metabolism in CNS. Bull Exp Biol Med 2017;163:307–312.
42. Garde E, Lykke Mortensen E, Rostrup E, Paulson OB. Decline in intelligence is associated with progression in white matter hyperintensity volume. J Neurol Neurosurg Psychiatry 2005;76:1289–1291.
43. Lockhart SN, Mayda AB, Roach AE, et al. Episodic memory function is associated with multiple measures of white matter integrity in cognitive aging. Front Hum Neurosci 2012;6:56.
44. Aizenstein HJ, Nebes RD, Meltzer CC, et al. The relation of White Matter Hyperintensities to implicit learning in healthy older adults. Int J Geriatr Psychiatry 2002;17:664–669.
45. Wardlaw JM, Valdés Hernández MC, Muñoz-Maniega S. What are White Matter Hyperintensities made of?: relevance to vascular cognitive impairment. J Am Heart Assoc 2015;4:e001140.
46. Soriano-Raya JJ, Miralbell J, López-Cancio E, et al. Tract-specific fractional anisotropy predicts cognitive outcome in a community sample of middle-aged participants with white matter lesions. J Cereb Blood Flow Metab 2014;34:861–869.
47. Ramirez J, McNeely AA, Berezuk C, et al. Dynamic Progression of White Matter Hyperintensities in Alzheimer's disease and normal aging: results from the Sunnybrook Dementia Study. Front Aging Neurosci 2016;8:62.
48. Longstreth WT Jr, Manolio TA, Arnold A, et al. Clinical correlates of white matter findings on cranial magnetic resonance imaging of 3301 elderly people. The Cardiovascular Health Study. Stroke 1996;27:1274–1282.
49. Wang GJ, Volkow ND, Logan J, et al. Brain dopamine and obesity. Lancet 2001;357:354–357.
50. Kaffashian S, Dugravot A, Elbaz A, et al. Predicting cognitive decline: A dementia risk score vs the Framingham vascular risk scores. Neurology 2013;80:1300–1306.

